J. Anat. (2006) **209**, pp699–705 doi: 10.1111/j.1469-7580.2006.00642.x

Magnetic resonance imaging of the Harderian gland in piglets

Berit H. Munkeby,[1,3,4] Hans-Jørgen Smith,[2,4] Eldrid H. Winther-Larssen,[2] Atle Bjørnerud[2,4] and Inge Bjerkås[5]

[1]*Department of Pediatric Research,* [2]*Department of Radiology,* [3]*Institute for Surgical Research, Rikshospitalet-Radiumhospitalet Medical Center,* [4]*University of Oslo, Oslo, Norway*
[5]*Norwegian School of Veterinary Science, Oslo, Norway*

Abstract

The main purpose of the present study was to investigate the value and effectiveness of functional and morphological magnetic resonance imaging (MRI), in order to assess the extent of brain injury in a hypoxic–ischaemic piglet model, and further to validate that the ischaemic injury was successfully induced. In this way, we also characterized the Harderian gland. MRI was performed at 1.5 T in anaesthetized piglets (n = 10, 12–36 h of age). Magnetic resonance perfusion and diffusion imaging were performed at different time points, before, during and after the induction of hypoxia–ischaemia. The effects following bilateral clamping of the carotid arteries were also assessed by contrast-enhanced magnetic resonance angiography. Morphological assessment included T1- and T2-weighted imaging, and fat-suppressed T1-weighted imaging before and after contrast medium enhancement. Morphological MRI revealed a prominent, well-defined structure located at the eyeball. Magnetic resonance angiography reconstructed with volume rendering showed this structure to be partially enclosed by large venous sinuses. At dissection, when compared with the magnetic resonance images, the deep gland of the third eyelid, the Harderian gland, corresponded to this structure both in topography and in size. By contrast, the lacrimal gland proper presented as a small, soft and pale structure that was difficult to distinguish from the surrounding connective tissue. At histological examination, the Harderian gland consisted mainly of compact areas of tubuloacinar glands with abundant eosinophilic granules. The present MRI demonstration of the Harderian gland was an accidental finding during an investigation to assess the extent of brain injury in a hypoxic–ischaemic piglet model. The combination of MRI and histology made it possible to detect and describe the Harderian gland in pig. It has generally been studied in rodents and lower vertebrates and is reported to possess various endocrine and exocrine functions.

Key words Harderian gland; histology; morphological MRI; MR angiography; piglet; T1- and T2-images.

Introduction

Over 300 years ago, the Swiss physician and anatomist Johann Jakob Harder reported his discovery of a glandula nova lachrymalis in deer, suggesting that the large structure he had identified served to moisten the surface of the eye (Harder, 1694).

It is now referred to as the Harderian gland (HG, glandula profunda palpebrae tertiae), and is located within the orbit of terrestrial vertebrates that exhibit a nictitating membrane (palpebra tertia) (Sbarbati et al. 2002). The anatomical location within the orbit and the size of the HG vary among species. Despite more than three centuries of study, many features of this gland, including its definition and function, are not yet established.

The HG is found to possess various endocrine as well as exocrine functions (Sbarbati et al. 2002). The functions of the gland are protection and lubrication of the cornea, a site of immune responses, a source of pheromones and a source of thermoregulatory lipids (Payne, 1994).

The HG has been described in different species, including the rabbit (Ulbrich, 1910; Davis, 1929), mouse

Correspondence
Berit Holthe Munkeby, Department of Pediatric Research, Rikshospitalet-Radiumhospitalet Medical Center, University of Oslo, Norway.
T: +47 23 07 27 93; F: +47 23 07 27 80; E: b.h.munkeby@medisin.uio.no

Accepted for publication *29 June 2006*

(Yamashita, 1980), rat (Greene, 1968; Timm, 1979; Hebel & Stromberg, 1986), golden hamster (Pansky et al. 1961), reptiles, amphibians and birds (Ortiz, 2001; Sbarbati et al. 2002). Adult humans do not have a HG, but HG vestiges seem to be present in the human fetus between weeks 11 and 30 (Buzzell, 1996).

The HG gland also exists in the pig (Ellenberger & Baum, 1906; Nickel et al. 1975), which is widely used as an experimental animal in human research (Hraste et al. 1995).

In the pig, the HG gland has not previously been described using magnetic resonance imaging (MRI) and, apart from macroscopic descriptions in veterinary anatomical textbooks, further reports on histology and function are sparse in the literature. As with other animals with a third eyelid, the pig also has a superficial accessory lacrimal gland (glandula superficialis, nictitating gland) in addition to the lacrimal gland proper (glandula lacrimalis), which is located dorsolateral to the eyeball. The pig is one of the few animals to possess both an HG and a nictitating gland (Prince et al. 1960).

Much of our current understanding concerning human neonatal physiology derives from studies conducted in animal models (Myers, 1977), and a large body of data has been gathered in the newborn pig. Their anatomy and physiology are in many respects close to those of humans (Tumbleson, 1986; Swindle et al. 1988; Hannon et al. 1990; Roohey et al. 1997).

The present paper reports findings from basic MRI studies in connection with an investigation of the suitability of functional and morphological MRI to assess the extent of brain injury in a hypoxic–ischaemic (HI) piglet model, and further to validate that the ischaemic injury was successfully induced (Munkeby et al. 2004). The results were correlated with those obtained using a sectional approach and by light microscopy.

Materials and methods

The experimental protocol was approved by the hospital's ethics committee for animal studies under the surveillance of the Norwegian Animal Research Authority, and performed by certified category C researchers of the Federation of European Laboratory Animal Science Associations.

Animal model

Newborn Landrace piglets (n = 10, age 12–36 h) were delivered from a local farmer (1 h transportation) on the day of the experiment. The piglets were anaesthetized, tracheotomized and mechanically ventilated (Munkeby et al. 2004). The anaesthesia, fluid replacement and monitoring were maintained as described previously (Munkeby et al. 2004). At the end of the experiment, the piglets were given an overdose of 150 mg kg^{-1} pentobarbital i.v.

Experimental model

After 1 h stabilization the piglets were subjected to 30 min of hypoxia, 8% O_2 in N_2 (AGA, Oslo, Norway), and bilateral clamping of the common carotid arteries, followed by 150 min reoxygenation with ambient air (21% O_2) and reperfusion. Both functional and structural MRI were performed before, during and after (30 and 150 min) the induction of HI. The various MR sequences used are described in detail below.

Magnetic resonance imaging

The anaesthetized piglets were imaged in the prone position using a 1.5-T scanner (Siemens Vision Plus, Erlangen, Germany) and a quadrature extremity coil. The imaging protocol was primarily designed to assess early neonatal brain injury, as previously described (Munkeby et al. 2004).

Morphological T2- and T1-weighted images of the piglet brain and orbits were obtained in an oblique coronal plane with respect to the brain. T2-weighting was acquired using a turbo spin echo sequence (TR/TE = 4500 ms/96 ms, voxel size = $0.4 \times 0.4 \times 3$ mm^3), and T1-weighting was obtained with a spin echo technique (TR/TE = 500 ms/12 ms, voxel size = $0.5 \times 0.5 \times 4$ mm^3). The T1-weighted sequence was repeated with fat suppression both before and after injection of an intravascular ultrasmall superparamagnetic iron oxide contrast agent (NC100150 Injection, Amersham Health, Oslo, Norway) at a dose of 4.5 mg Fe kg^{-1}. The contrast medium was also used for acquisition of contrast-enhanced MR angiography (MRA) of the head and neck with a three-dimensional spoiled gradient echo sequence (3D FLASH, TR/TE = 4.4 ms/1.8 ms, voxel size = $0.9 \times 0.9 \times 1.5$ mm^3). MR angiograms were reconstructed using maximum intensity projection and volume rendering.

Tissue preparation

Orbital structures of five pigs were dissected for correlation with the MR images. After dissection, the

materials from two pigs were stored in Keyserling's fluid and later photographed.

Materials for histology were obtained from the different lacrimal glands, and fixed in 10% buffered formalin and subsequently processed for light microscopy. Histological sections were stained with haematoxylin and eosin (HE), van Gieson-Hansen (VGH), Periodic acid Schiff (PAS) and Sudan black B. In addition, material from the Harderian gland was frozen in liquid nitrogen and sections stained with Oil red O for demonstration of lipids.

Results

Magnetic resonance imaging

Morphological MRI clearly identified two intraorbital spherical masses located ventromedial to the eyeballs. These masses, later defined as the HGs, had low signal intensity at T2-weighting (Fig. 1A–C) and high signal intensity at T1-weighting, both with and without fat suppression (Fig. 2A,B). They were partially surrounded by a vascular sinus, shown with high signal intensity at T2-weighting (Fig. 1A) and intense enhancement after injection of the intravascular contrast agent (Fig. 2C). The glands themselves showed no enhancement. MRA reconstructed with volume rendering showed the ophthalmic sinuses to be cup-shaped with an anterolateral opening for the HGs (Fig. 3). The HGs and the surrounding vascular sinus bordered medially on the olfactory bulb above and the ethmoidal conchae below (Fig. 1A–D). Just ventral to the glands and ophthalmic sinuses, the maxillary teeth could be seen (Fig. 1A–D). The HG had a diameter about half that of the eyeball. In the particular piglet illustrated (Figs 1–3), it had cross-sectional diameters of approximately 10.0×6.5 mm, as compared with the largest diameter of the eyeballs of 16.5 mm, and the largest cross-sectional diameters of the olfactory bulbs of 10.5×8.0 mm.

Gross anatomy

At dissection, when compared with the MR images, both the topography and the size of the deep gland of the third eyelid corresponded to the spherical mass seen on MRI (Fig. 4). It was thick, brownish and finely lobulated, and extended from the cartilage of the third eyelid towards the origin of the extrinsic eye muscles at the apex of the orbit (Fig. 4). By contrast, the superficial accessory lacrimal gland and the lacrimal gland proper presented as thin, softer and relatively pale structures that were difficult to distinguish from the surrounding connective tissue.

Histology

At histological examination, the HG presented as a very compact tubuloacinar gland arranged in lobules and with a distinct outline (Fig. 4E,F). The interlobular septa were thin and the intralobular connective tissue was likewise sparse and exhibited a fine capillary network around the tubuloacinar structures. Centrally in each lobule was an area of branching collecting tubules and vessels. The acini had a relatively large lumen, and the acinar cells contained numerous eosinophilic granules, which were strongly positive under PAS staining. Generally, the granules were most numerous in the apical part of the cells, but in some acini they filled the whole cells. Some acini also contained cells with less eosinophilic cytoplasm and larger nuclei, and with smaller granules. However, it could not be confirmed definitively whether these cells represented a different cell type or a different secretory stage. Sudanophilic granules were not demonstrated in the acinar cells; however, in frozen sections, fine Oil red O-positive granules were seen in epithelial cells of the collecting tubules. Both mitoses and apoptosis-like changes were seen. The surface capsule was covered with a very thin wall of a surrounding vascular space, which in one side was bridged by connective tissue that carried vessels and nerves to the gland.

The lacrimal gland proper (Fig. 4D) and the superficial gland of the third eyelid (Fig. 4E) were less distinctly outlined and consisted of more loosely arranged tubuloacinar structures with more abundant interstitial connective tissue. The acinar cells were weakly basophilic and contained no visible secretory granules in HE sections, but numerous strongly PAS-positive granules. There was no evidence of surrounding vascular sinuses.

Discussion

The HGs in the pig are clearly identified by MRI and are revealed to be circumscribed intraorbital structures of the eyeballs. The glands have remarkably high signal intensity at T1-weighting, indicating fast T1-relaxation, and moderately low signal intensity at T2-weighting, indicating an intermediate T2-value. A short T1-value is

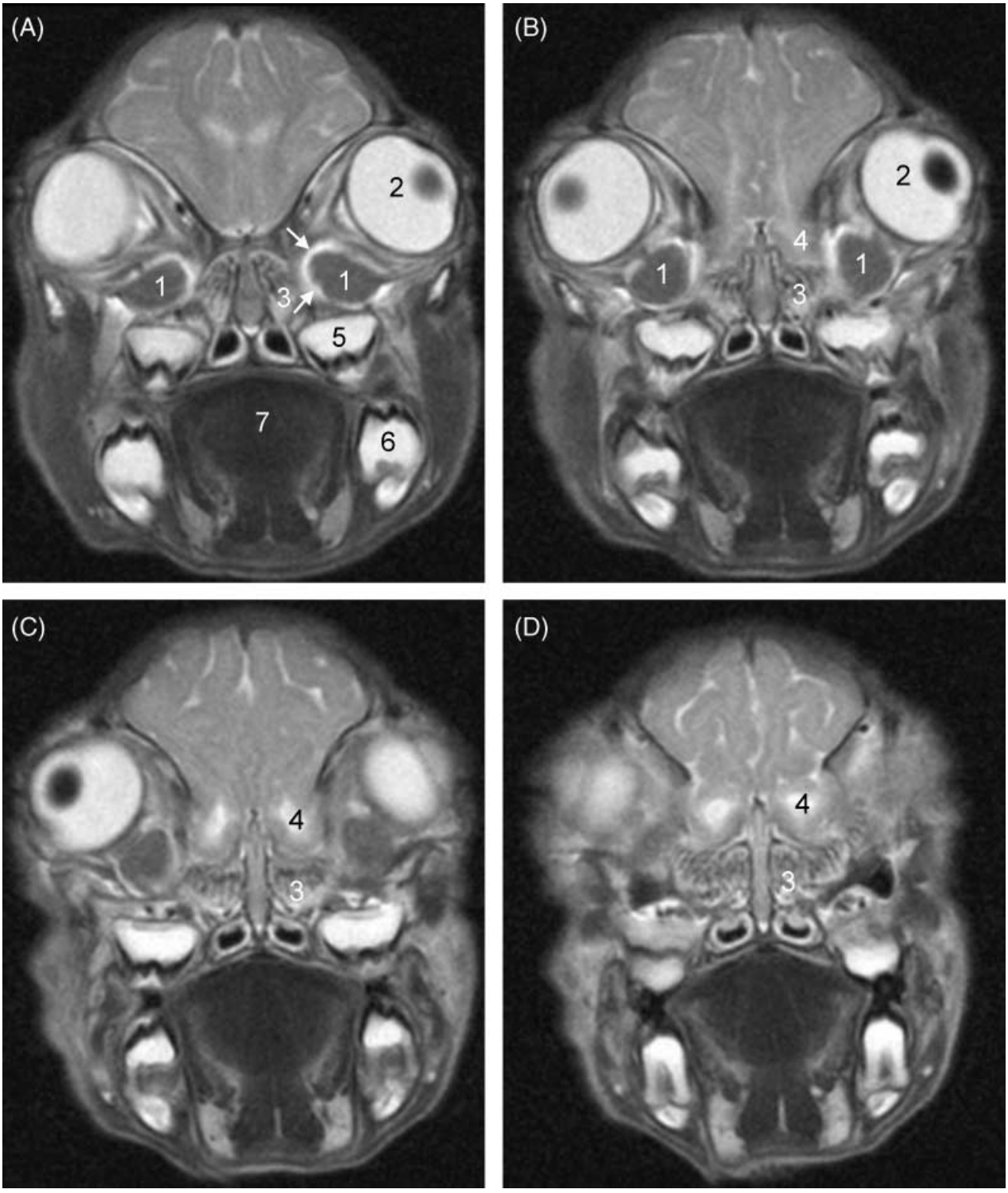

Fig. 1 T2-weighted oblique coronal MR images through the anterior orbits from posterior (A) to anterior (D). Three-millimetre-thick consecutive slices with 0.3-mm interslice gaps are shown. 1: Harderian glands; 2: left eyeball with (dark) lens; 3: left ethmoidal conchae; 4: left olfactory bulb; 5: tooth, left upper jaw; 6: tooth, left lower jaw; 7: tongue. White arrows: high-intensity rim representing ophthalmic sinus.

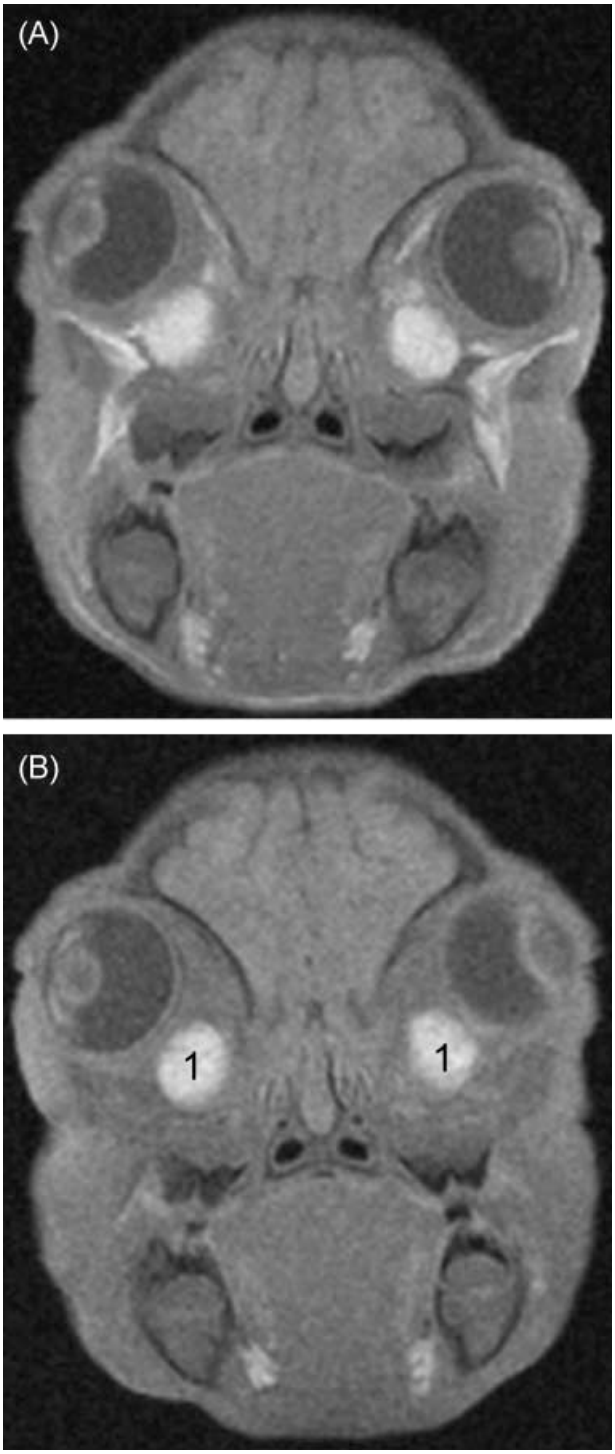

Fig. 2 Oblique coronal T1-weighted (A), fat-suppressed T1-weighted (B), and post-contrast fat-suppressed T1-weighted (C) MR images of the same piglet as in Fig. 1. The Harderian glands (1) are shown with high signal intensity before and after contrast medium injection. There is intense contrast enhancement of the ophthalmic sinuses (arrows) partially surrounding the glands.

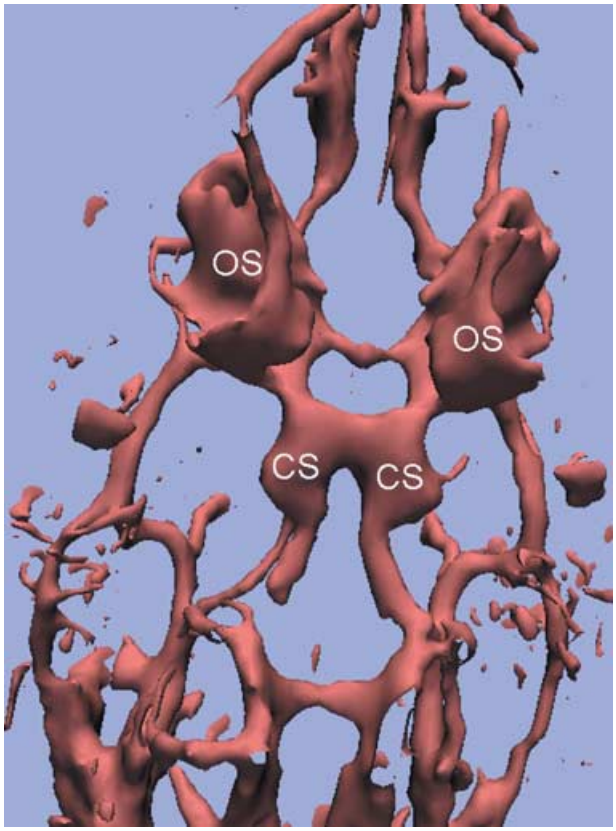

Fig. 3 MR angiography of the orbital and skull base vessels reconstructed with volume rendering. The cup-shaped ophthalmic sinuses (OS) enclosing the Harderian glands (not shown) are seen from the dorsal side of the piglet head. CS: cavernous sinus surrounding the rete mirabile.

characteristic of fatty tissue, haemorrhage (due to methaemoglobin), proteinaceous fluids and the presence of paramagnetic compounds. The high signal intensity at T1-weighting with fat suppression rules out fatty tissue as a cause of the short T1-relaxation. In humans, the combination of high signal intensity at fat-suppressed T1-weighting and intermediate low signal intensity at T2-weighting is typical of normal pancreatic tissue. In fact, no other human organs show these imaging characteristics. The short T1 of normal pancreatic parenchyma has been attributed to the exocrine proteinaceous fluid, the rich endoplasmatic reticulum and the high content of paramagnetic manganese ions in the acinar cells. It seems possible that a similar mechanism may be true for the HG in pigs, suggesting that the short T1-value is related to the exocrine function of the acinar cells. Like the exocrine pancreas, the pig HG has a sparse stroma, and the acinar cells contain numerous eosinophilic secretory granules. There

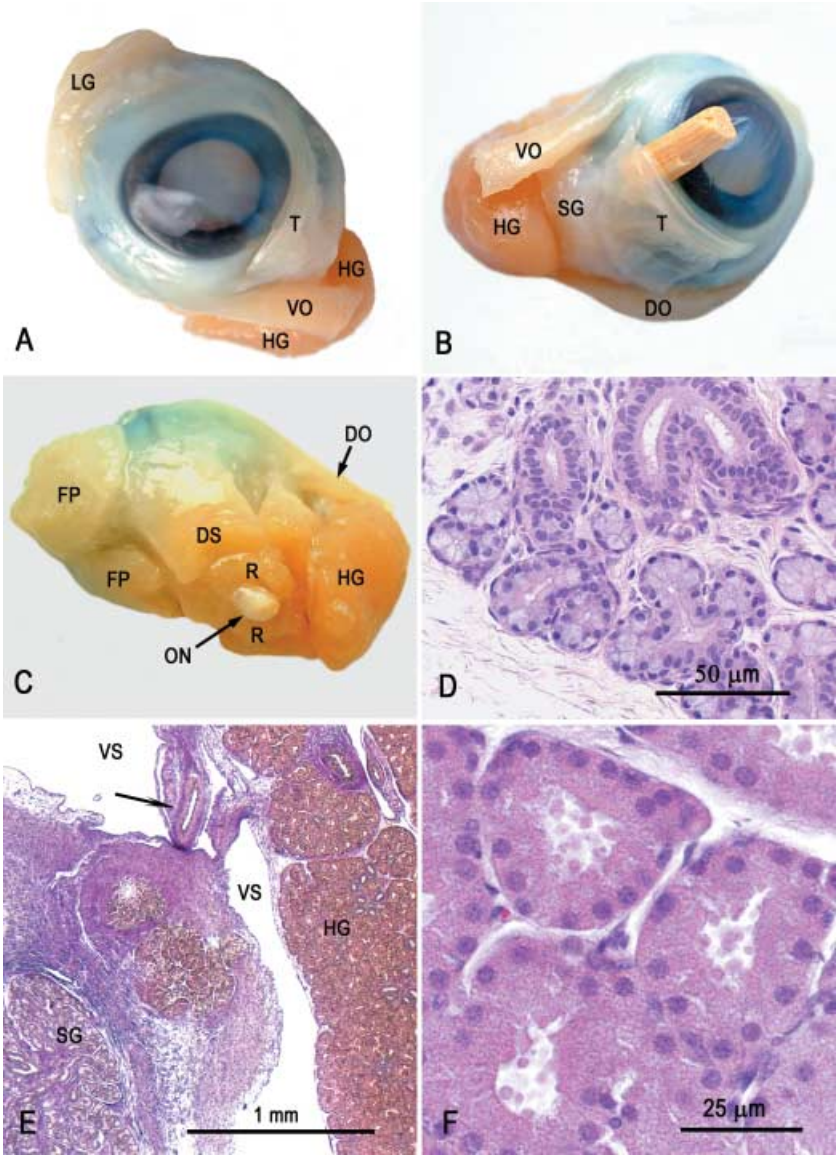

Fig. 4 Dissected left eye with adnexa, fixed in Keyserling's fluid (A–C), and histological sections of the lacrimal gland proper (D) and Harderian gland (E, F). DO, dorsal oblique muscle; DS, dorsal straight muscle; FP, fat pad; HG, Harderian gland; LG, lacrimal gland; ON, optic nerve; R, retractor bulbi muscle; SG, superficial gland of third eyelid; T, third eyelid; VO, ventral oblique muscle; VS, vascular sinus. (A) Anterior view. Note the difference in size and colour between the lacrimal and Harderian glands. (B) Medioventral view. The superficial gland of the third eyelid is clearly seen. A piece of a match is placed beneath the third eyelid to make it more distinct. (C) Posterior view. The posterior extent of the Harderian gland is shown. (D) Histological section of the lacrimal gland proper. Note the abundant interstitial connective tissue and the lack of a distinct capsule. HE staining. (E) The Harderian gland presents as a compact area to the right, and is mostly separated from the base of the third eyelid by a vascular space bridged by vessels and nerves (arrow). The superficial gland of the third eyelid is seen at the lower left corner. VGH staining. (F) Eosinophilic acini of the Harderian gland with granular content. HE staining.

are indications that they contain acid mucopolysaccharides (Hraste et al. 1995), but further knowledge of the contents of the pig HG seems to be lacking. In other species a wide variety of substances has been reported (Ortiz, 2001). Compared with the other lacrimal glands, the Harderian gland had a more compact structure with less interacinar connective tissue.

The present MR images as well as the histological sections showed that the HG was for the most part separated from the surrounding tissues by a vascular sinus. Simoens (1985) has shown that the HG of pigs is surrounded by the rostroventral section of a venous enlargement termed the sinus ophthalmicus (Diesem, 1975). Arteria palpebrae tertiae (from a. malaris of a. ophthalmica interna) penetrates the rostroventral section of the ophthalmic sinus, and here it gives rise to several branches to the HG. In each side, the ophthalmic sinus connects via the vena emissaria foraminis orbitorotundi with the sinus cavernosus, which surrounds the rete mirabile epidurale rostrale.

We have demonstrated that the HG in the newborn pig is of a considerable size, and larger than the lacrimal gland. To our knowledge there are still no published studies on the fine structure and functions of the HG in pig.

Conclusion

The present MRI demonstration of the HG was an accidental finding during an investigation to assess the

extent of brain injury in an HI piglet model. In pigs, this gland has received little attention in the literature compared with the other species mentioned herein. However, taking its size into consideration, it must be of significant importance also in the pig. It has generally been studied in rodents and lower vertebrates and has been found to possess various endocrine and exocrine functions.

Acknowledgements

This work was supported by a grant from the Norwegian SIDS Society, the Laerdal foundation for Acute Medicine, the University of Oslo, AGA AB Medical Research Fund and the Norwegian Society of Anaesthesiology.

References

Buzzell GR (1996) The Harderian gland: perspectives. *Microsc Res Techn* **34**, 2–5.

Davis FA (1929) The anatomy and histology of the eye and orbit of the rabbit. *Trans Am Ophthalmol Soc Annu Meeting* **27**, 401–441.

Diesem CD (1975) The organ of vision. In *Sisson and Grossman's the Anatomy of the Domestic Animals* (ed. Getty R), pp. 1409–1417. Philadelphia: W.B. Saunders Company.

Ellenberger W, Baum H (1906) *Handbuch der Vergleichenden Mikroskopischen Anatomie der Haustiere*. Berlin: Paul Parey.

Greene EC (1968) Glands of the orbit. In *Anatomy of the Rat* (ed. Greene EC), pp. 1–370. New York: Hafner.

Hannon JP, Bossone CA, Wade CE (1990) Normal physiological values for conscious pigs used in biomedical research. *Lab Anim Sci* **40**, 293–298.

Harder JJ (1694) Glandula nova lachrymalis una cum ductu excretorio in cervis et damis. *Acta Eruditorum Lipsiae*, 49–52.

Hebel R, Stromberg MW (1986) *Anatomy and Embryology of the Laboratory Rat*. Wörthsee: BioMed.

Hraste A, Gjurcevic Kantura V, Jokovac M, Jukic Brestovec J (1995) Morphological investigations of the glandulae profundae plicae semilunares conjuctivae in the domestic swine (*Sus scrofa domesticus*) and the wild hog (*Sus scrofa ferus*). *Anat Histol Embryol* **24**, 223–226.

Munkeby BH, Lyng K, Froen JF, et al. (2004) Morphological and hemodynamic magnetic resonance assessment of early neonatal brain injury in a piglet model. *J Magn Reson Imaging* **20**, 8–15.

Myers R (1977) Experimental models of perinatal brain damage: relevance to human pathology. In *Intrauterine Asphyxia and the Developing Fetal Brain* (ed. Gluck L), pp. 37–97. Chicago: Year Book Medical.

Nickel R, Schummer A, Seiferle E (1975) *Lehrbuch der Anatomie der Haustiere*. Berlin: Verlag Paul Parey.

Ortiz GG (2001) Different patterns in the histology and autofluorescence of the Harderian glands of the Syrian Hamster, rat, mouse, Mongolian gerbil and guinea pig. *Anat Histol Embryol* **30**, 107–115.

Pansky B, Jacobs M, House E, Tassoni J (1961) The orbital region as a source of blood samples in the golden hamster. *Anat Rec* **139**, 409–412.

Payne AP (1994) The harderian gland: a tercentennial review. *J Anat* **185**, 1–49.

Prince JH, Diesem CD, Eglitis I, Ruskell GL (1960) The pig. In *Anatomy and Histology of the Eye and Orbit in Domestic Animals* (ed. Prince JH), pp. 210–233. Springfield, IL: Charles C Thomas.

Roohey T, Raju TN, Moustogiannis AN (1997) Animal models for the study of perinatal hypoxic-ischemic encephalopathy: a critical analysis. *Early Hum Dev* **47**, 115–146.

Sbarbati A, Calderan L, Nicolato E, et al. (2002) Magnetic resonance imaging of the rat Harderian gland. *J Anat* **201**, 231–238.

Simoens P (1985) *Morphologic Study of the Vasculature in the Orbit and Eyeball of the Pig*. Ghent: State University of Ghent, Faculty of Veterinary Medicine.

Swindle MM, Smith AC, Hepburn BJ (1988) Swine as models in experimental surgery. *J Invest Surg* **1**, 65–79.

Timm K (1979) Orbital venous anatomy of the rat. *Lab Anim Sci* **29**, 636–638.

Tumbleson M (1986) *Swine in Biomedical Research*. New York: Plenum.

Ulbrich H (1910) Die venöse Blutsinus in der Orbita des Kaninchens. *Arch Augenheilkunde* **65**, 179–188.

Yamashita T (1980) Spatial aspect of the mouse orbital venous sinus. *La Reforme Sociale* **56**, 329–336.